NeuroImage: Clinical 19 (2018) 911–917

Contents lists available at ScienceDirect

NeuroImage: Clinical

journal homepage: www.elsevier.com/locate/ynicl

# Temporal lobe epilepsy lateralization using retrospective cerebral blood volume MRI

Xinyang Feng[a], Marla J. Hamberger[b], Hannah C. Sigmon[b], Jia Guo[a], Scott A. Small[b,c,*], Frank A. Provenzano[b,c,*]

[a] Department of Biomedical Engineering, Columbia University, New York, NY, United States
[b] Department of Neurology, College of Physicians and Surgeons, Columbia University, New York, NY, United States
[c] Taub Institute for Research on Alzheimer's Disease and the Aging Brain, Columbia University, New York, NY, United States

ARTICLE INFO

*Keywords:*
Cerebral hemodynamics
Cortical mapping
Epilepsy
Hippocampus
MRI

ABSTRACT

Steady-state cerebral blood volume (CBV) is tightly coupled to regional cerebral metabolism, and CBV imaging is a variant of MRI that has proven useful in mapping brain dysfunction. CBV derived from exogenous contrast-enhanced MRI can generate sub-millimeter functional maps. Higher resolution helps to more accurately interrogate smaller cortical regions, such as functionally distinct regions of the hippocampus. Many MRIs have fortuitously adequate sequences required for CBV mapping. However, these scans vary substantially in acquisition parameters. Here, we determined whether previously acquired contrast-enhanced MRI scans ordered in patients with unilateral temporal lobe epilepsy can be used to generate hippocampal CBV. We used intrinsic reference regions to correct for intensity scaling on a research CBV dataset to identify white matter as a robust marker for scaling correction. Next, we tested the technique on a sample of unilateral focal epilepsy patients using clinical MRI scans. We find evidence suggestive of significant hypometabolism in the ipsilateral-hippocampus of unilateral TLE subjects. We also highlight the subiculum as a potential driver of this effect. This study introduces a technique that allows CBV maps to be generated retrospectively from clinical scans, potentially with broad application for mapping dysfunction throughout the brain.

## 1. Introduction

Magnetic resonance imaging (MRI) has an increasingly evolving clinical role in neurology for both disease diagnosis, assessment of therapeutic response and surgical planning (Matthews et al., 2006). Growing clinical investigation and adoption of these imaging methods continue as more research confirms analytic and methodological approaches. For instance, blood oxygenation level dependent fMRI (BOLD) imaging was recently evaluated by the American Academy of Neurology and defined as a way to evaluate memory and language lateralization with certain epilepsy patients in lieu of the more traditional and invasive approach, the intracarotid amobarbital procedure (IAP) (Szaflarski et al., 2017). While fMRI is frequently used to refer to BOLD-only variants of brain imaging, there are several technically functional MRI methods that can reveal information that may be clinically useful, including exogenous contrast CBV, vascular space occupancy (VASO) CBV, arterial spin labelling (ASL), and diffusion MRI (Donahue et al., 2006; Haacke et al., 2015).

Cerebral blood volume (CBV) is a measure of the quantity of blood in a unit of tissue (Petrella and Provenzale, 2000). A variant of MRI generated from steady-state exogenous contrast brain imaging using intravenous contrast agent can be used to generate CBV values on a voxel by voxel basis (Lin et al., 1999). Values of percent CBV extracted from these scans have been shown to reflect a basal state cerebral activity, and similarly, CBV has been shown to strongly correlate to 18-flourodeoxyglucose positron emission tomography (FDG-PET), an otherwise accepted imaging measurement reflective of glucose metabolism (González et al., 1995). However, there are inherent assumptions made regarding in vivo detection measurements and corresponding extracted quantitative values. For instance, FDG-PET measures glucose uptake, and any assumptions of metabolism correlates are based on the coupling of glucose uptake and otherwise uniform and unaffected astrocytic functioning (Magistretti and Pellerin, 1996).

At its core, what distinguishes this variant of CBV from other functional MRI measures is that the requisite scans require the introduction of contrast agent. This method provides higher spatial and lower temporal resolution compared to dynamic variants of fMRI, in

* Corresponding authors at: 630 W 168th Street PH 18-400, New York, NY 10032, United States.
*E-mail addresses:* sas68@columbia.edu (S.A. Small), fap2005@columbia.edu (F.A. Provenzano).

https://doi.org/10.1016/j.nicl.2018.05.012
Received 16 January 2018; Received in revised form 27 April 2018; Accepted 9 May 2018
Available online 10 May 2018

addition to an increase in intravascular signal to noise ratio (SNR) (Lin et al., 1999). Contrast agent is used clinically to reveal signal changes reflective of oncological or inflammatory origin, as well as other underlying pathologies; however, the majority of clinically ordered contrast-enhanced scans reflect intact vasculature (radiologically noted as "non-contrast enhancing"). As such, any steady state cortical signal change after contrast enhancement is likely to reflect the passive (venule and capillary) component of blood capacity, whereas dynamic CBV measurements, such as VASO, would likely capture arterial and arteriolar changes (Kim and Kim, 2011).

For research steady state exogenous contrast CBV MRI scans, the post-contrast image and pre-contrast image must be in the same intensity translation and scaling system in order to accurately calculate the contrast uptake and determine voxel level CBV values. Dynamic ranges of the signal in pre-contrast and post-contrast acquisition may vary, especially if parameters related to the MRI voxel signal values and intensities are left to scanner default parameters (as is common for MRI scanners unless otherwise specified). Differences in manufacturing, scanner software versioning and sequences have been shown to introduce variability in cortical thickness estimations, though the variability has not been well characterized as much in the clinical domain (Han et al., 2006). Changes in signals before and after contrast enhancement may potentially cause disparate signal ranges between scan instances, precluding an accurate estimation of relative change in contrast uptake. In certain experimental practices, an external intensity fiducial marker may be scanned at the same time to help with intermodal co-registration (Woods et al., 1993). Additionally, the intensity of the fiducial marker may be used to correct gross image intensity differences (Simor et al., 1995). However, for most scan sessions, there are no external fiducial markers. In these scenarios, there is not a straightforward way to correct the image for potential quantitative steady state exogenous contrast CBV processing. This study proposes a method whereby reference regions may be used to overcome this obstacle as it relates to analyses requiring intensity preservation.

Millions of contrast enhanced MRI scans are performed annually in the United States for a variety of indications including lesion enhancement, malignancies or inflammation (Lohrke et al., 2016). Many of the protocols for these scans overlap with the protocols of the requisite scans necessary for research CBV. Given the glut of scans acquired for myriad clinical reasons, we aimed to determine whether functional measures can be extracted from these previously "unused" scans, potentially to a clinically informative end. To do so we needed to both develop a method to simulate and correct potential confounds in retrospective analyses and forward apply it to a dataset with known dysfunction.

As previously discussed, most of current imaging modalities reflecting proxy metabolic measurements, including PET, ASL, and dynamic susceptibility contrast (DSC-MRI) have limited whole-brain spatial resolution using standard machines and procedures, rarely at or below 1 mm, which is the anatomical basis for most cortical segmentation algorithms. Additionally, studies on hippocampal subfields are primarily carried out in structural, T1 and T2 weighted MRI. Providing that a majority of the scans have resolution comparable to resolutions used for FreeSurfer's hippocampal subfield segmentation algorithm, we can examine the mean CBV values of hippocampal subfields.

We wish to explore our scaling correction method on a study of temporal lobe epilepsy (TLE) lateralization using MRI scans acquired for surgical evaluations. TLE is a seizure disorder in which the region of seizure onset can lateralize to either the left or right temporal lobe, or can involve the temporal lobes, bilaterally. For pharmacologically refractory patients who are potentially candidates for surgical treatment, lateralization of the epileptogenic zone is essential, and presents a challenge in the context of an unremarkable clinical structural MRI scan. Temporal lobe epilepsy laterality has been studied using many different imaging modalities including PET (Sarikaya, 2015; Theodore et al., 1997), ASL (Wolf et al., 2001), and DSC-MRI (Wu et al., 1999) for metabolism studies and structural MRI for structural studies (Mueller et al., 2009). The purpose of this analysis is two-fold and uses two distinct data sets: a CBV research dataset, acquired from previous studies with appropriate acquisition and scaling parameters defined on the MRI prior to scan acquisition and a TLE clinical dataset, onto which we will evaluate our scaling correction method and potentially test for functional lateral differences; specifically, CBV decreases ipsilateral to the side of seizure onset. In addition, we would like to interrogate the sub-regions of the hippocampus within this TLE group. We hope that this study may provide some potential insight into the pathophysiology of the hippocampal circuit in epilepsy using an approach that can be retrospectively and prospectively applied to patients who would receive these scans regardless.

## 2. Material and methods

### 2.1. Data

We included 304 pairs of correctly scaled pre-contrast scans and post-contrast scans in the study acquired from a collection of studies for which CBV MRI scans were included. This collection of images includes a broad population of subjects across different studies and age ranges, including follow-up scans of the same subjects. Both healthy subjects and subjects with various diseases, including schizophrenia, post-traumatic stress disorder, Alzheimer's disease, are included. The scans were acquired using a high-resolution T1-weighted gradient echo sequence as previously described (Brickman et al., 2014; Khan et al., 2014). Example slices of pre-contrast image, post-contrast image, derived difference image, and ratio image are shown in Fig. 1. The image intensity statistics of representative tissue types including cerebral grey matter (GM), cerebral white matter (WM), lateral ventricle cerebrospinal fluid (CSF), and pure blood in superior sagittal sinus as annotated in the figure are listed in Table S2 in the supplementary material.

In this study, the CBV research dataset is used only to determine an appropriate reference region (or reference region combination) that is unlikely to reflect potential lateralized signal changes.

For the retrospective study on epilepsy, 34 unilateral TLE patients with pre-contrast and post-contrast T1-weighted scans were screened from an internal database via retrospective chart review from 2011 to 2016. The laterality was determined based on video-scalp EEG recording of seizure onset with no evidence of seizures arising from the contralateral hemisphere. Other inclusion criteria include age $> 18$ and IQ $> 70$. Predicting a similar level of effect, the number of patients included exceeds an existing study demonstrating potential hypometabolism effect (Wolf et al., 2001). Four patients were excluded from study due to space-occupying hippocampal lesions as noted by a radiologist through clinical evaluation. Four additional patients were excluded due to MRI technical issues including significant mismatch of MRI acquisition parameters of pre and post-contrast scans (one case: pre-contrast image TE 3 ms TR 16.67 ms, post-contrast image TE 5 ms TR 19 ms), severe artifact, prohibitive field of view (one case: FOV of pre-contrast scan not covering brain posterior to corpus callosum) or inadequate segmentation. The list of scanning parameters can be found in Table S1 in the supplementary material. Among the remaining scans, only one set of scans were acquired using a 1.5 T scanner (last row in Table S1). We excluded that subject for the sake of data homogeneity. The exclusion process for MRI technical issues was blind to patient diagnosis information. The receiver gain calibration was on for each pair of scans. Mesial temporal sclerosis (MTS) is not an exclusion criterion in this study, 5/26 patients have MTS. It should be noted that MTS is likely to be a common coincident finding in TLE (Liu et al., 2012).

The Columbia University Institution Review Board (IRB), which abides by the guidelines outlined in the Declaration of Helsinki of 1975, approved retrospective analysis of clinical MRI scans, in addition to all subjects' providing explicit written consent at the time of scanning to

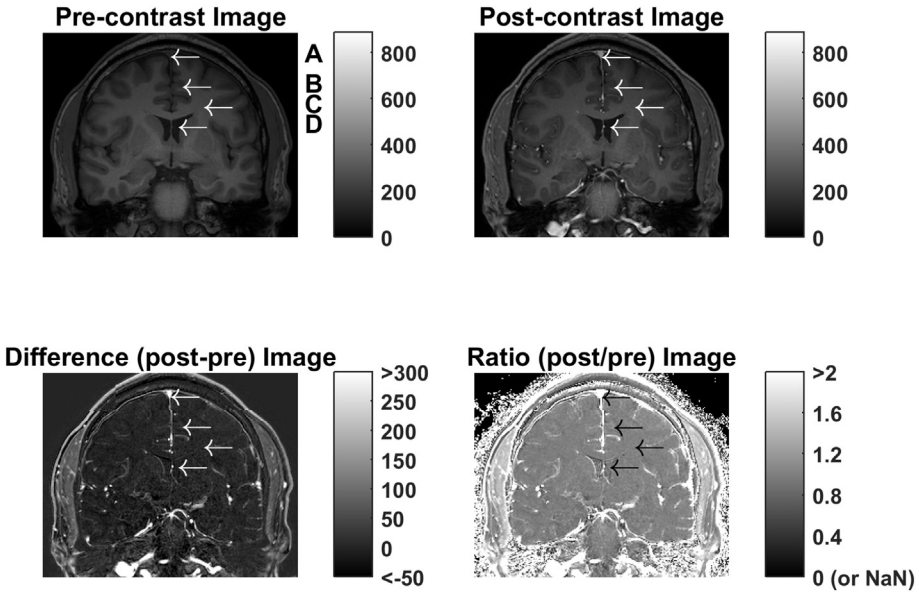


**Fig. 1.** An illustration of the pre-contrast image, post-contrast image, the difference (post-pre) image, and the ratio (post/pre-contrast) image on a coronal slice in a correctly-scaled pair of images. The image intensity statistics for representative tissue types, including cerebral GM (B), cerebral WM (C), lateral ventricle CSF (D), and pure blood in superior sagittal sinus (A) are calculated and listed in Table S2. The statistics are calculated based on $5 \times 5$ voxel regions; the centres of the squares are pinpointed by the arrows.

participate in research studies.

A diagram demonstrating both the research and clinical databases and streams is shown in Figure SM1 in the supplementary material.

### 2.2. Scaling correction factor estimation with brain region segmentation

The first step in attempting to identify a way to correct scaling within clinical scans is to align each of the clinical scans intensity. Borrowing the idea from external fiducial marker, we expected there might be an appropriate internal reference region relatively unaffected by contrast, which would be resilient to post-contrast signal change. In that case, the ratio of the intensity value of post-contrast image to pre-contrast image in the region of interest (ROI) would approach 1.

The pre-contrast images are segmented using FreeSurfer (Fischl et al., 2002; Van Leemput et al., 2009) with the hippocampal subfield segmentation applied. All scans were quality checked by a trained reviewer. The post-contrast image was co-registered to the pre-contrast image through intra-subject linear co-registration using FSL FLIRT with six degrees of freedom and correlation ratio cost function (Jenkinson et al., 2002). Although both scans are of the same sequence parameters, we considered the presence of contrast enhancement to require a cost function befitting an inter-modal registration versus intra-modal registration. The FreeSurfer segmentation masks were also resliced to the pre-contrast image space. The segmentation masks were applied to the pre-contrast and co-registered post-contrast images. Mean values for post/pre-contrast ratio values within ROIs were computed and used as features for subsequent processing.

Forty-five regions are segmented and labelled. To further refine the results, only regions with at least 100 voxels across scans are regarded robust and valid, which results in 38 regions remaining. As shown in Fig. 2 in the Results section, every region has increased signal with respect to the application of contrast agent.

Ideally, a region wholly unaffected by contrast uptake could be used to correct scaling. However, there is no consistent region within the brain with unequivocal preservation of signal. As such, we wish to find a region that can be consistently segmented with the lowest signal change e.g. coefficient of variation. WM would be expected to have the lowest based on its known cerebrovasculature. The coefficient of variation for cerebral WM (both left and right) post/pre-contrast ratio is the smallest of all the regions (shown in Fig. 2 in the Results section).

### 2.3. Scaling correction factor estimation with tissue class segmentation

Since the values of white matter show consistency across scans, we explored the post/pre-contrast ratio on coarser segmentations by only segmenting the brain into different tissue types, WM, GM and CSF instead of different anatomical regions. This provides an advantage in computational time and robustness, which is very important for large-scale applications.

The pre-contrast image is first brain extracted using FSL BET (Smith, 2002). The brain extraction image is then segmented into WM, GM, and CSF using FSL FAST (Zhang et al., 2001). To exclude the possible influence of GM on WM, the WM mask was eroded using a morphological 3-dimensional kernel. The post/pre-contrast ratio for each tissue type is generated the same way as described in the previous section.

The ratios for all the scans in the training set are fitted to a normal distribution separately for each tissue type (or region). For a new test scan, the same processing steps are implemented, generating ratio for each tissue type. The ratios are substituted into the probability distribution functions fitted using the training set, generating normalized likelihood. Each ratio can be used to predict the scaling correction factor (SCF): $SCF_R = \hat{\mu}_R / r_R$, where $\hat{\mu}_R$ denotes the mean ratio value of the tissue $R$ in the training set; $r_R$ denotes the ratio value for tissue $R$ from the new scan.

### 2.4. Generating relative CBV map

The pre-contrast image was subtracted from the co-registered, scaling corrected post-contrast image to generate a raw subtracted image. The raw subtracted image was normalized by the mean value of grey matter to generate the relative CBV (rCBV) map. Detailed information can be found in Supplemental Methods.

### 2.5. Joint region combining

The scaling correction can be more robust through joint regional combining using the likelihoods calculated in the above sections especially when underlying pathologies exist that would impact or alter the tissue class segmentation or properties. For more information, see Supplemental Methods.

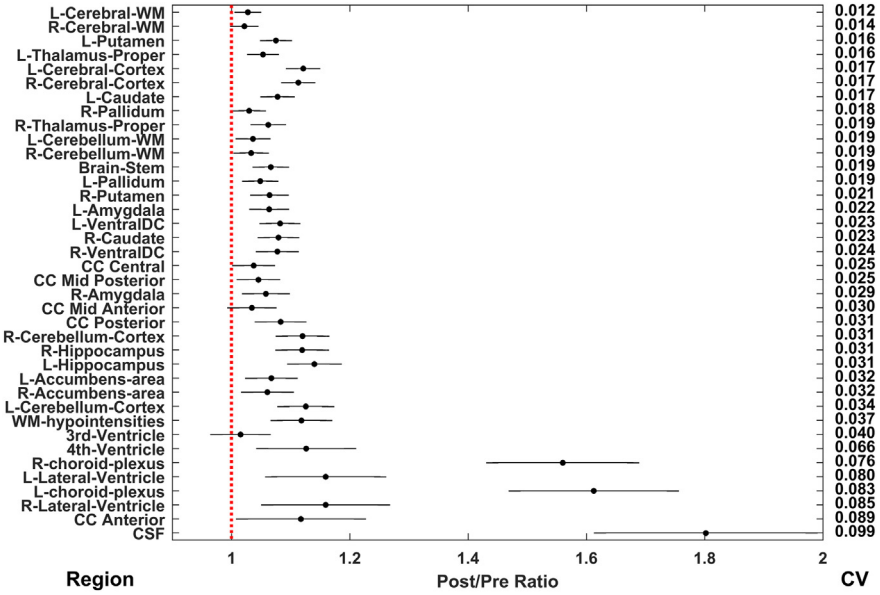


**Fig. 2.** Post/pre-contrast ratio values (mean ± standard deviation) for regions from FreeSurfer automatic subcortical segmentation pipeline. The regions are sorted in the order of the coefficient of variation (CV) of post/pre-contrast ratio.

### 2.6. Retrospective TLE analysis

We applied the scaling correction method using the WM segmentation from FAST on the TLE data and measured the rCBV in hippocampus and hippocampal subfields. We analyse the CBV SNR by calculating the mean CBV divided by the standard deviation within white matter. A reference distribution was established on research CBV MRI scans. The difference of contralateral and ipsilateral rCBV was used to study the epilepsy lateralization. We examined CA1, CA3, dentate gyrus (DG), pre-subiculum (PRE-SUB), and subiculum (SUB) hippocampal subfields. In the individual analysis, raw data were first visualized with boxplots, and outliers were excluded outside of 1.5 times the interquartile range (IQR) for a given distribution.

## 3. Results

### 3.1. Screening internal reference region

The results of screening using FreeSurfer segmentation are shown in Fig. 2 and suggest that there is not an unaffected anatomically well-defined region with a ratio distributed around 1 in the FreeSurfer segmentation protocol. The scaling correction factor for each scan was estimated in leave-one-out manner. The lowest mean squared error 0.00014, mean absolute error 0.00888 and standard deviation 0.01193 are achieved with left cerebral WM alone.

The statistics of the estimated scaling correction factors using WM, GM, and CSF ratios alone and using the combinations can be found in Table S3 in the supplementary material. Using WM provides the best estimation regarding mean absolute error (0.00998), mean squared error (0.00017); whereas WM/CSF achieves slightly lower standard deviation (0.01292) and similar mean squared error (0.00017). The mean squared error, mean absolute error, and standard deviation levels are close to those achieved using regional segmentations.

### 3.2. Retrospective TLE analysis

All clinical scans lie within two standard deviation of the mean of the reference SNR distribution of our existing database. We found a statistically significant relative CBV decrease in the hippocampus ipsilateral to seizure-onset (one-tailed paired $t$-test, $N_{Left\text{-}TLE} = 17$, $N_{Right\text{-}TLE} = 6$, $p < 0.05$) with a mean contralateral ipsilateral difference 0.082 (standard deviation, 0.174) (See Fig. 3). This finding is in line with previous studies suggesting ipsilateral hypometabolism in mesial temporal lobe using PET (Sarikaya, 2015; Theodore et al., 1997), ASL (Wolf et al., 2001) and DSC-MRI (Wu et al., 1999). The result is significant when examining the left TLE patients ($N_{Left\text{-}TLE} = 17$, $p < 0.05$) and trending when examining the right TLE patients ($N_{Right\text{-}TLE} = 6$, $p = 0.055$) alone.

We found statistically significant mean rCBV change in the ipsilateral subiculum (one-tailed paired $t$-test, $N_{Left\text{-}TLE} = 15$, $N_{Right\text{-}TLE} = 6$, $p < 0.01$, surviving multiple comparison correction with $N_{Comparison} = 5$) with a mean contralateral ipsilateral difference 0.177 (standard deviation, 0.289) (See Fig. 4). We found no significant differences in hippocampal volumes or hippocampal subfield volumes (one-tailed paired $t$-tests, $p > 0.05$).

We also compared the directional relative metabolic asymmetry (rCBV right side–rCBV left side). This analysis looks at subject differences in subtracted hippocampal rCBV values between the left and right TLE groups. We found a significant difference in left-TLE and right-TLE in the hippocampus (one-tailed $t$-test, $N_{Left\text{-}TLE} = 17$, $N_{Right\text{-}TLE} = 6$, $p < 0.05$) and subiculum (one-tailed $t$-test, $N_{Left\text{-}TLE} = 15$, $N_{Right\text{-}TLE} = 6$, $p < 0.01$, surviving multiple comparison correction with $N_{Comparison} = 5$) within hippocampal subfields. The results can be found in Fig. S1 and Fig. S2 in supplementary material.

## 4. Discussion

In MRI scans that were acquired both intentionally and unintentionally for CBV analysis, we demonstrate that tissue segmentation based methods can achieve accurate scaling correction. WM plays the primary part in the estimation. The use of white matter as reference region is also supported by a brain volume study for potential technical advantage (Maclaren et al., 2014), where cerebral white matter volume was shown to have the least measurement variation. However, in the event this method was to be used in a cohort with suspected WM signal change like WM lesions or potential demyelinating diseases, this estimation model can incorporate other tissue classes to improve the robustness potentially mediated by non-uniform WM.

Physiologically speaking, the white matter and cerebrospinal fluid should uptake little gadolinium; while grey matter is more densely vascularized leading to increased contrast uptake. The different uptake within the GM tissue class across regions across scans renders the ratio

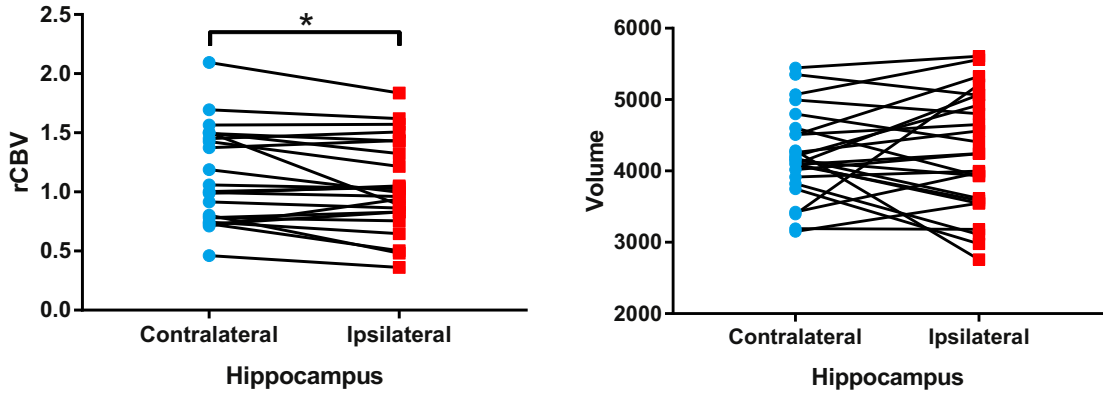


**Fig. 3.** The rCBV (left) and volume (right) of hippocampus contralateral and ipsilateral to the seizure onset. We find statistically significant ipsilateral rCBV decrease but not significant structural difference for hippocampus.

of GM more variant than WM, which already may vary across modality of CBV, reflecting either a systematic anatomic (venous versus arterial) difference or scaling difference (Lu et al., 2005; Sourbron et al., 2009). Segmentation accuracy and partial volume effects may also contribute to this variance, though would likely affect the entire image uniformly. The segmentation of GM is likely to include regions of both micro and macro vasculature, which reflects the greatest contrast after contrast agent application. Though in principle, CSF uptakes little gadolinium; the segmentation of CSF may be prone to the influence of vasculature or GM. This is one reason for the relatively high average ratio and high variance for CSF. The mean intensity ratio calculated using the eroded WM masks is similar to the value using the uneroded WM mask, which suggests a relative consistent distribution of gadolinium uptake across the periphery of the white matter and robust segmentation of white matter.

Although a number of studies have shown lateralized hippocampal volume differences in TLE versus other epilepsy types (Marsh et al., 1997), we found no significant lateral differences in hippocampal volume in our TLE cohort. This likely related to the small proportion of TLE patients with MTS in our sample (i.e., < 20%), as reduced hippocampal volume would be expected, primarily in patients with MTS (Carne et al., 2004; Mueller et al., 2009). Unlike patients with unilateral TLE and ipsilateral MTS who show ipsilateral versus contralateral differences in hippocampal volume, non-lesional TLE patients without MTS tend not to show these differences.

### 4.1. Finer segmentation of white matter

As white matter shows better homogeneity among the regions, we further explored the finer structure of cerebral white matter using the FreeSurfer parcellation results. There are 178 common labels for all the scans including 38 labels in the automatic subcortical segmentation results, 70 labels for the cortical parcellation, and 70 corresponding labels for the white matter parcellation. For the voxels in white matter, the label is assigned as the nearest cortical parcellation label (Salat et al., 2009). As the number of labels is relatively large, the result is not shown here graphically. The top structures with least variant post/pre-contrast ratio are all white-matter structures. The results further support the consistency of white matter regarding the post/pre-contrast ratio; though, the minimum coefficient of variation is not significantly smaller than using white matter as a whole.

### 4.2. Epilepsy lateralization

Refractory TLE patients with structurally normal MRI scans often present a challenge to the surgical team with regard to lateralization of seizure onset. Our results suggest that CBV measurements may provide supportive information regarding the laterality of the epileptogenic region. Future studies may explore the role of CBV MRI in lieu of PET scanning, as CBV would require no additional scanning beyond clinically acquired MRI protocols requiring contrast enhanced imaging. Additionally, our work suggests the subiculum could be a driver of the metabolic dysfunction, supporting existing research on the subiculum's

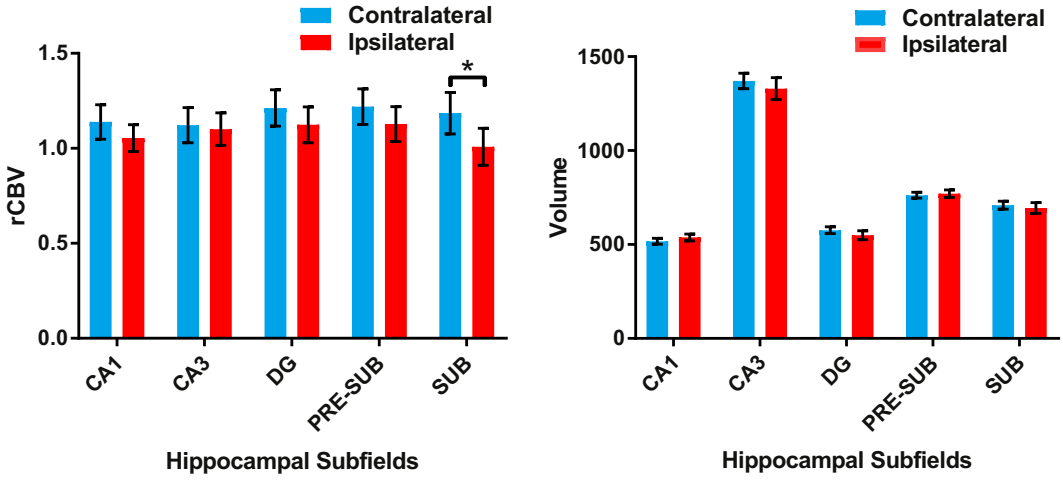


**Fig. 4.** The rCBV (left) and volume (right) of hippocampal subfields contralateral and ipsilateral to the seizure onset. We find statistically significant ipsilateral rCBV decrease in subiculum but no significant structural asymmetry for hippocampal subfields. The error-bars show the standard error of the mean.

role in epileptogenesis (Stafstrom, 2005). Electrophysiological studies on extracted hippocampal lesions in TLE have implicated the subiculum as the potential origin of interictal activity (Cohen et al., 2002). One possible explanation may be a result of a loss of afferent CA1 interneurons. Although we found no significant changes in the CA1 subfields, this could be due to potential subtle sclerotic changes affecting the accuracy of subfield segmentation.

### 4.3. Limitations

For inter-subject analysis, it would be important to process all of the data in the same pipeline, as there is systematic bias using different methods (Klauschen et al., 2009). The validity of the method depends on the stability of the within-method variation. Given the choices of software and methods of publically available software, FAST and FreeSurfer are likely to provide accurate and reproducible results for this analytical stream (Valverde et al., 2015). With regards to FreeSurfer segmentations not revealing an unaffected region for contrast, it is possible that other structures (such as air-filled paranasal sinuses) otherwise not defined in the segmentation template used in this study could be potentially accurate internal reference regions.

Additionally, bias field is often a concern for brain MRI processing and can systematically affect the intensity value in a large scale. The influence of bias field and other MRI artefacts is under further investigation. However, since bias field is generally assumed multiplicative based on the underlying physics (Sled et al., 1998), it is not predicted to have impacted the ratio values. However, further study would be needed across scanners and head coils.

By using relative CBV, we are assuming the absence of global change in CBV. Although hemispheric global grey matter CBV changes are unlikely, it would be important to examine those mean values more carefully to ensure that those do not inaccurately affect the results.

## 5. Conclusions

In this study, we provide evidence for ipsilateral hippocampal CBV changes in patients with unilateral TLE using intensity corrected steady state contrast enhanced CBV functional MRI. This was achieved with an analytical stream that was agnostic of scanner brand, type and protocol and can be rewritten to be semi-automated or potentially implemented in an informatics network or system. Since these scans were acquired not for an imaging research study but for potential pre-surgical evaluation, this work demonstrates the potential of this framework to characterize the cerebral functional profile of patients who may have retrospectively acquired these scans. Similarly, this analysis permits the ability for high-resolution metabolic maps to be generated using scans that would already be acquired as a matter of clinical course and evaluation. This applies not only to focal hippocampal metabolic dysfunction, but also to any indication where MR imaging with contrast is standard or warranted. This analysis and methodological investigation serves as an example of how newer analytical approaches may serve as a lens to refocus scan protocols to generate clinically relevant imaging measures. Additionally, future studies may focus on hippocampal subregional analysis and cognitive correlates, as certain sub-regions have been shown to exhibit selective vulnerability in different disease states.

## Author contribution statement

XF, HCS, JG and FP obtained data. XF performed image analysis. XF, FP and SS prepared manuscript. MH recruited subjects and proposed hypothesis.

## Disclosures

FAP is a co-founder and has equity in IMIJ technologies. SAS has equity in and/or serves on the board of Denali Therapeutics and IMIJ technologies.

## Acknowledgements

The authors wish to thank the Taub Institute MRI Pilot Platform grant (MH) and the American Epilepsy Society Seed grant AES2017SD2 (MH).

## Appendix A. Supplementary data

Supplementary data to this article can be found online at https://doi.org/10.1016/j.nicl.2018.05.012.

## References

Brickman, A.M., Khan, U.A., Provenzano, F.A., Yeung, L.K., Suzuki, W., Schroeter, H., Wall, M., Sloan, R.P., Small, S.A., 2014. Enhancing dentate gyrus function with dietary flavanols improves cognition in older adults. Nat. Neurosci. 17, 1798–1803.
Carne, R.P., O'Brien, T.J., Kilpatrick, C.J., MacGregor, L.R., Hicks, R.J., Murphy, M.A., Bowden, S.C., Kaye, A.H., Cook, M.J., 2004. MRI-negative PET-positive temporal lobe epilepsy: a distinct surgically remediable syndrome. Brain 127, 2276–2285.
Cohen, I., Navarro, V., Clemenceau, S., Baulac, M., Miles, R., 2002. On the origin of interictal activity in human temporal lobe epilepsy in vitro. Science 298, 1418–1421.
Donahue, M.J., Lu, H., Jones, C.K., Edden, R.A., Pekar, J.J., van Zijl, P.C., 2006. Theoretical and experimental investigation of the VASO contrast mechanism. Magn. Reson. Med. 56, 1261–1273.
Fischl, B., Salat, D.H., Busa, E., Albert, M., Dieterich, M., Haselgrove, C., Van Der Kouwe, A., Killiany, R., Kennedy, D., Klaveness, S., 2002. Whole brain segmentation: automated labeling of neuroanatomical structures in the human brain. Neuron 33, 341–355.
González, R.G., Fischman, A.J., Guimaraes, A.R., Carr, C.A., Stern, C.E., Halpern, E.F., Growdon, J.H., Rosen, B.R., 1995. Functional MR in the evaluation of dementia: correlation of abnormal dynamic cerebral blood volume measurements with changes in cerebral metabolism on positron emission tomography with fludeoxyglucose F 18. Am. J. Neuroradiol. 16, 1763–1770.
Haacke, E.M., Liu, S., Buch, S., Zheng, W., Wu, D., Ye, Y., 2015. Quantitative susceptibility mapping: current status and future directions. Magn. Reson. Imaging 33, 1–25.
Han, X., Jovicich, J., Salat, D., van der Kouwe, A., Quinn, B., Czanner, S., Busa, E., Pacheco, J., Albert, M., Killiany, R., Maguire, P., Rosas, D., Makris, N., Dale, A., Dickerson, B., Fischl, B., 2006. Reliability of MRI-derived measurements of human cerebral cortical thickness: the effects of field strength, scanner upgrade and manufacturer. NeuroImage 32, 180–194.
Jenkinson, M., Bannister, P., Brady, M., Smith, S., 2002. Improved optimization for the robust and accurate linear registration and motion correction of brain images. NeuroImage 17, 825–841.
Khan, U.A., Liu, L., Provenzano, F.A., Berman, D.E., Profaci, C.P., Sloan, R., Mayeux, R., Duff, K.E., Small, S.A., 2014. Molecular drivers and cortical spread of lateral entorhinal cortex dysfunction in preclinical Alzheimer's disease. Nat. Neurosci. 17, 304–311.
Kim, T., Kim, S.G., 2011. Quantitative MRI of cerebral arterial blood volume. Open Neuroimaging J. 5, 136–145.
Klauschen, F., Goldman, A., Barra, V., Meyer-Lindenberg, A., Lundervold, A., 2009. Evaluation of automated brain MR image segmentation and volumetry methods. Hum. Brain Mapp. 30, 1310–1327.
Lin, W., Celik, A., Paczynski, R.P., 1999. Regional cerebral blood volume: a comparison of the dynamic imaging and the steady state methods. J. Magn. Reson. Imaging 9, 44–52.
Liu, M., Concha, L., Lebel, C., Beaulieu, C., Gross, D.W., 2012. Mesial temporal sclerosis is linked with more widespread white matter changes in temporal lobe epilepsy. Neuroimage Clin. 99–105.
Lohrke, J., Frenzel, T., Endrikat, J., Alves, F.C., Grist, T.M., Law, M., Lee, J.M., Leiner, T., Li, K.C., Nikolaou, K., Prince, M.R., Schild, H.H., Weinreb, J.C., Yoshikawa, K., Pietsch, H., 2016. 25 years of contrast-enhanced MRI: developments, current challenges and future perspectives. Adv. Ther. 33, 1–28.
Lu, H., Law, M., Johnson, G., Ge, Y., van Zijl, P., Helpern, J.A., 2005. Novel approach to the measurement of absolute cerebral blood volume using vascular-space-occupancy magnetic resonance imaging. Magn. Reson. Med. 54, 1403–1411.
Maclaren, J., Han, Z., Vos, S.B., Fischbein, N., Bammer, R., 2014. Reliability of brain volume measurements: a test-retest dataset. Sci. Data 1.
Magistretti, P.J., Pellerin, L., 1996. The contribution of astrocytes to the $^{18}$F-2-deoxyglucose signal in PET activation studies. Mol. Psychiatry 1, 445–452.
Marsh, L., Morrell, M.J., Shear, P.K., Sullivan, E.V., Freeman, H., Marie, A., Lim, K.O., Pfefferbaum, A., 1997. Cortical and hippocampal volume deficits in temporal lobe epilepsy. Epilepsia 38, 576–587.
Matthews, P.M., Honey, G.D., Bullmore, E.T., 2006. Applications of fMRI in translational medicine and clinical practice. Nat. Rev. Neurosci. 7, 732–744.
Mueller, S.G., Laxer, K.D., Barakos, J., Cheong, I., Garcia, P., Weiner, M.W., 2009. Subfield atrophy pattern in temporal lobe epilepsy with and without mesial sclerosis detected by high-resolution MRI at 4 Tesla: preliminary results. Epilepsia 50, 1474–1483.
Petrella, J.R., Provenzale, J.M., 2000. MR perfusion imaging of the brain: techniques and applications. AJR Am. J. Roentgenol. 175, 207–219.
Salat, D.H., Greve, D.N., Pacheco, J.L., Quinn, B.T., Helmer, K.G., Buckner, R.L., Fischl, B., 2009. Regional white matter volume differences in nondemented aging and

Alzheimer's disease. NeuroImage 44, 1247–1258.
Sarikaya, I., 2015. PET studies in epilepsy. Am. J. Nucl. Med. Mol. Imaging 5, 416–430.
Simor, T., Chu, W.-J., Johnson, L., Safranko, A., Doyle, M., Pohost, G.M., Elgavish, G.A., 1995. In vivo MRI visualization of acute myocardial ischemia and reperfusion in ferrets by the persistent action of the contrast agent Gd (BME-DTTA). Circulation 92, 3549–3559.
Sled, J.G., Zijdenbos, A.P., Evans, A.C., 1998. A nonparametric method for automatic correction of intensity nonuniformity in MRI data. IEEE Trans. Med. Imaging 17, 87–97.
Smith, S.M., 2002. Fast robust automated brain extraction. Hum. Brain Mapp. 17, 143–155.
Sourbron, S., Ingrisch, M., Siefert, A., Reiser, M., Herrmann, K., 2009. Quantification of cerebral blood flow, cerebral blood volume, and blood–brain-barrier leakage with DCE-MRI. Magn. Reson. Med. 62, 205–217.
Stafstrom, C.E., 2005. The role of the subiculum in epilepsy and epileptogenesis. Epilepsy Curr. 5, 121–129.
Szaflarski, J.P., Gloss, D., Binder, J.R., Gaillard, W.D., Golby, A.J., Holland, S.K., Ojemann, J., Spencer, D.C., Swanson, S.J., French, J.A., Theodore, W.H., 2017. Practice guideline summary: use of fMRI in the presurgical evaluation of patients with epilepsy: report of the Guideline Development, Dissemination, and Implementation Subcommittee of the American Academy of Neurology. Neurology 88, 395–402.
Theodore, W.H., Sato, S., Kufta, C.V., Gaillard, W.D., Kelley, K., 1997. FDG-positron emission tomography and invasive EEG: seizure focus detection and surgical outcome. Epilepsia 38, 81–86.
Valverde, S., Oliver, A., Cabezas, M., Roura, E., Lladó, X., 2015. Comparison of 10 brain tissue segmentation methods using revisited IBSR annotations. J. Magn. Reson. Imaging 41, 93–101.
Van Leemput, K., Bakkour, A., Benner, T., Wiggins, G., Wald, L.L., Augustinack, J., Dickerson, B.C., Golland, P., Fischl, B., 2009. Automated segmentation of hippocampal subfields from ultra-high resolution in vivo MRI. Hippocampus 19, 549–557.
Wolf, R.L., Alsop, D.C., Levy-Reis, I., Meyer, P.T., Maldjian, J.A., Gonzalez-Atavales, J., French, J.A., Alavi, A., Detre, J.A., 2001. Detection of mesial temporal lobe hypoperfusion in patients with temporal lobe epilepsy by use of arterial spin labeled perfusion MR imaging. AJNR Am. J. Neuroradiol. 22, 1334–1341.
Woods, R.P., Mazziotta, J.C., Cherry, S.R., 1993. MRI-PET registration with automated algorithm. J. Comput. Assist. Tomogr. 17, 536–546.
Wu, R.H., Bruening, R., Noachtar, S., Arnold, S., Berchtenbreiter, C., Bartenstein, P., Drzezga, A., Tatsch, K., Reiser, M., 1999. MR measurement of regional relative cerebral blood volume in epilepsy. J. Magn. Reson. Imaging 9, 435–440.
Zhang, Y., Brady, M., Smith, S., 2001. Segmentation of brain MR images through a hidden Markov random field model and the expectation-maximization algorithm. IEEE Trans. Med. Imaging 20, 45–57.